BUILDING AND ENVIRONMENT

Simulation-based Assessment of A S H R A E Guideline 36, Considering Energy Performance, Indoor Air Quality, and Control Stability

Cary A. Faulkner[a], Robert Lutes[b], Sen Huang[c], Wangda Zuo[d,e], Draguna Vrabie[b]

[a]University of Colorado Boulder, Boulder, CO, USA
[b]Pacific Northwest National Laboratory, Richland, WA, USA
[c]Oak Ridge National Laboratory, Oak Ridge, TN, USA
[d]Pennsylvania State University, University Park, PA, USA
[e]National Renewable Energy Laboratory, Golden, CO, USA

A B S T R A C T
  This study assesses American Society of Heating, Refrigerating and Air-Conditioning Engineers Guideline 36 (G36) with a typical medium ofice building. Specifically, this study modified a Modelica model of a variable air volume (VAV) system that serves this building, which is a part of the Building Operations Testing (B O P T E S T) Framework, by introducing components for representing indoor virus transmission and filtration. It then implemented the G36 control sequences for both water-side and air-side equipment in Python. After that, this study conducted the assessment by co-simulating G36 and the Modelica model using the B O P T E S T Framework. Unlike existing works, this work has three unique features: 1)It considers the interactions between control sequences for water-side and air-side equipment of the studied VAV system. 2)It assesses the performance of G36 from the perspective of IAQ. 3)It examines the short-term behaviors of the studied building under G36 to understand the control stability. This assessment confirms significant energy savings from G36, largely because of the interaction between supply air temperature and hot water controls. It also reveals a trade-off between the ability to slow the spread of virus and the energy performance via demand controlled ventilation. Lastly, it emphasizes the necessity of tuning local feedback control when implementing G36.

1. Introduction

Advanced building control (A B C) has been recognized as a research priority [1]. A B C addresses the challenges of operating modern buildings, such as the inherent nonlinearity of the building dynamics [2] and the conflicting nature of the operating objectives [3]. According to a survey conducted in [4], the application of A B Cs can effectively improve the enabled energy savings and thermal comfort, which commonly conflict with each other, under various nonlinear operating conditions. As a result, significant research efforts have been devoted to develop and test A B Cs, as summarized in [5].

Corresponding Author: Sen Huang. Email: huangs@ornl.gov

Among those efforts, the works on developing and promoting American Society of Heating, Refrigerating and Air-Conditioning Engineers (ASHRAE) Guideline 36: High-Performance Sequences of Operation for HVAC Systems (G36) [6] have attracted increasing attention. G36 is designed to provide uniform sequences of operation for heating, ventilation, and air conditioning (HVAC) systems. It is based on the outputs of several research projects, including ASHRAE Research Project 1455 Advanced Control Sequences for HVAC Systems - Phase I Air Distribution and Terminal Systems [7], ASHRAE Research Project 1711 Advanced Sequences of Operation for HVAC Systems – Phase II Central Plants and Hydronic Systems [8], and a research project [9] conducted by National Institute of Standards and Technology (NIST). In 2018 and 2021, ASHRAE released the first version (G36_2018) and the second version (G36_2021) of G36, respectively. G36_2018 contains only the control sequences for air-side HVAC equipment, such as variable air volume (VAV) terminals, while G36_2021 also includes sequences for hydronic HVAC systems and additional air-side HVAC equipment.

Despite promising results regarding the energy performance of G36 in [10], the real-world adoption of G36 is still slow. One reason is the lack of a comprehensive assessment of the overall performance of G36. Relevant studies in the literature have limited ability to provide such an assessment , as elaborated in Section 2.3.

To address these gaps, this work presents a simulation-based evaluation of G36_2021 (referred as G36 hereinafter) in this paper with a typical medium ofice building system. Specifically, this work leveraged a Modelica [11] model of a VAV system that serves this ofice building, which is from the Building Operations Testing (BOPTEST) Framework [12]. This Modelica model was modified by introducing models for indoor virus transmission and HVAC filtration to analyze the impact of G36 on different IAQ metrics. This work then implemented the G36 control sequences for both water-side and air-side equipment of this VAV system in Python [13]. Finally, a co-simulation of the implemented sequences and the Modelica model was set up via the BOPTEST Framework to conduct the control assessment. Unlike existing works, this work has three unique features:

- It considers the interactions between control sequences for water-side and air-side equipment of the studied VAV system.
- It assesses the performance of G36 from the perspective of IAQ.
- It examines the short-term behaviors of the studied building under G36 to understand the control stability.

The rest of the paper is organized as follows. Section 2 summarizes the existing studies in the literature and highlights the research gaps. Section 3 describes the control assessment, including implementation of G36, modifications of the Modelica model, defined performance metrics, and co-simulation settings. Section 4 presents the major results of the control assessment and the relevant discussions. Section 5 concludes this paper and envisions future work.

2. Literature Review

The existing works for testing and assessing G36 in the literature are categorize into two groups. The first group is field tests, where researchers studied G36 via implementation in real controllers, which serve either occupied or simulated buildings. Second are simulation tests, where researchers implement G36 in software and perform co-simulation of the control with simulated buildings. The field tests and the simulation

tests of G36 are summarized individually in the following sections.

2.1. Field Tests of ASHRAE Guideline 36

Ferretti et al. [14] implemented G36_2018 in the NIST Virtual Cybernetic Building Testbed, where the commercial building HVAC control equipment is linked to a building simulation model and the exterior environment. Then, Ferretti et al. conducted functional performance tests to determine the effectiveness of detecting faults and implementation errors.

Nassif [15] implemented the duct static pressure resetting algorithm of the G36_2018 in a BACnet web-based building automation system that serves a fully instrumented VAV system. Nassif then studied how the resetting algorithm affected the performance of VAV boxes in terms of the time of being starved and the fan energy savings.

Yoon et al. [16] implemented G36_2018 in a building management system that serves a two-story multi-zone unoccupied research apparatus. Their study validated that the implementation of G36_2018 resulted in expected behaviors of the testing VAV systems with a half-month test.

Field tests are straightforward and can usually yield the most accurate testing results as the testing conditions are close to the actual operation conditions of G36. On the other hand, those field tests also share the following drawbacks, preventing them from being deployed at a large-scale:

- It is expensive and labor-intensive to set up the field tests. All the field tests described above employed specific testing facilities. Those facilities require high initial costs associated with the purchase of equipment/software and/or building construction. They also require significant efforts to set up the channels on the data acquisition system to connect sensor inputs and control outputs.
- Field tests are not flexible when it comes to modifying the testing conditions. As not all the components in a field test are controllable, there are always limitations or constraints when expanding the testing scope. For example, tests typically must run in real time because of the use of real building control hardware. This can result in very long test times. Additionally, the lack of control over outdoor conditions can make it dificult to test the control under different operating scenarios.

2.2. Simulation Tests of ASHRAE Guideline 36

Pang et al. [17] implemented the occupant-centric building controls from both ASHRAE Standard 90.1 – 2019 [18] and G36_2018 in EnergyPlus [19] and performed simulations using the Department of Energy Commercial Prototype Building Models (DOE Prototype Models) [20]. Based on the simulation results, Pang et al. estimated a nation-wide energy saving potential from implementing the occupant-centric building controls.

Lee et al. [21] implemented the supply air temperature reset control (SAT reset) from G36_2018 in Python [22] and co-simulated the SAT reset with DOE Prototype Models to study how the energy performance of the SAT reset varies based on climate location.

Zhang et al. [10] implemented G36_2018 in the Control Description Language [23], a subset of the Modelica language, and simulated the G36_2018 control with an air handling system and building envelope model constructed using the Modelica Build-

3

ings library [24] to assess its energy performance. This study was then extended by Lu et al. [25] and Zhang et al. [26], respectively.

Lu et al. [25] included operation faults, such as sensor bias, in the simulation to understand how G36_2018 handled and adapted to those faults. Zhang et al. [26] enhanced the building envelope model with the Spawn of EnergyPlus technology [27].

Compared with field tests, simulation tests have two advantages: 1) they are less expensive to build as no hardware is involved and 2) they are more flexible since most of the variables in the simulation are controllable. On the other hand, the accuracy of the simulation tests is subject to the assumptions, which are inevitable when developing building energy simulations. For example, resetting of control setpoints may be assumed to be met during one simulation step, which ignores the short-term behaviors of those controllers. However, emerging technologies in building simulation during recent decades pave the way for the adoption of more accurate building models for control testing, which is also reflected in the reviewed papers [2]. For example, the simplified implementations of resetting controls of previous studies are replaced with more faithful representations in [26], which are able to capture the short-term dynamics due to changing setpoints.

2.3. Summary

Based on the above discussion, simulation tests are promising for supporting large-scale assessment of G36, primarily because of their low cost and higher flexibility. However, the existing simulation tests do not fully unleash the potentials of building simulation and have the following limitations:

- Only G36_2018 is studied in those tests. As mentioned in Section 1, G36_2018 only contains the control sequences for air-side HVAC equipment. In these cases, the control sequences for air-side HVAC equipment were assessed individually, without considering their potential interactions with other control sequences, such as those for water-side HVAC equipment. However, those interactions can be significant [28].
- Those tests studied the energy performance of G36 by comparing the energy consumption of the HVAC equipment under the control sequences from G36 to that of the HVAC equipment under different baseline controls. However, the impacts of G36 on building operation are limited to only energy performance. For example, it has been proven that building control may significantly affect IAQ [29]. Ignoring those non-energy impacts may lead to biased conclusions about G36.
- Most of those tests only considered the behaviors of the controlled HVAC equipment over a longer time period, e.g., a year. Nevertheless, when it comes to control evaluation, short-term performance, such as control stability [30], is also critical. In [21], Lee et al. found that the G36_2018 may cause the VAV terminal damper positions to oscillate. However, due to known issues in EnergyPlus that affect its ability to capture short-term building performance [31], these results may be interpreted qualitatively rather than quantitatively.

To resolve those limitations, this work considers G36_2021 which includes control sequences for both air-side HVAC equipment and hydronic HVAC systems. In addition, this work studies the performance of G36 in the context of virus scenarios, providing insights of how G36 impacts the IAQ. Finally, this work includes a high-fidelity building model, allowing to look into the short-term building operation under g36.

4

3. Methodology

Figure 1 illustrates the procedure for the control assessment of G36. This procedure consists of three steps:

- **ASHRAE Guideline 36 Implementation**
  This step implements the control sequences in G36 in a Python environment. It also defines the studied control sequences from G36 and specifies the underlying control logics for each individual control sequence. In this step, an empirical verification is also conducted to ensure desired control performance.
- **Building Model Development**
  This step defines the studied VAV system in terms of system configuration and local control loops. It considers the behaviors of the studied system, including long-term energy consumption, short-term responses of the HVAC equipment to the control actions, the indoor CO_2 concentrations, and the spread of virus. Finally, in this step, the studied VAV system is modeled in Modelica.
- **Control Evaluation**
  This step defines the evaluation metrics used to assess the performance of G36 from different aspects, including energy performance and IAQ. It also establishes a software setup to realize a co-simulation between Python and Modelica in runtime and specifies the detailed settings to run the simulation.
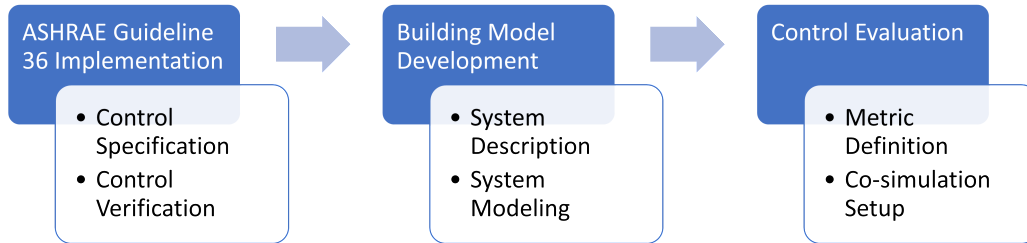

Figure 1.: Procedure for the control assessment of G36.

3.1. ASHRAE Guideline 36 Implementation

3.1.1. Control Specification

Five control sequences from G36_2021, as summarized in Table 1 are considered. These represent a comprehensive set of sequences for the studied multi-zone VAV system with an air-cooled chiller and air-cooled heat pump. The first four control sequences (duct static pressure reset, SAT reset, chilled water (CW) reset, and hot water (HW) reset) are based on a trim & respond logic, which is described in Algorithm 1. When using this trim & respond logic, the inputs (i.e., requests) are generated based on different control measurements for each sequence.

For the duct static pressure reset:

- If the measured airflow is less than 50% of setpoint while the setpoint is greater than zero and the damper position is greater than 95%, generate three requests.
- Else if the measured airflow is less than 70% of setpoint while the setpoint is greater than zero and the damper position is greater than 95%, generate two requests.

- Else if the damper position is greater than 95%, generate one request until the damper position is less than 85%.
- Else if the damper position is less than 95%, do not generate requests.

For the SAT reset:

- If the temperature exceeds its cooling setpoint by 3 °C, generate three requests.
- Else if the temperature exceeds its cooling setpoint by 2 °C, generate two requests.
- Else if the cooling signal is greater than 95%, generate one request until the cooling signal is less than 85%.
- Else if the cooling signal is less than 95%, do not generate requests.

For the CW reset:

- If the SAT exceeds its setpoint by 3 °C, generate three requests.
- Else if the SAT exceeds its setpoint by 2 °C, generate two requests.
- Else if the CW valve position is greater than 95%, generate one request until the CW valve position is less than 85%.
- Else if the CW valve position is less than 95%, do not generate requests.

For the HW reset:

- If the SAT is below its setpoint by 17 °C, generate three requests.
- Else if the SAT is below its setpoint by 8 °C, generate two requests.
- Else if the HW valve position is greater than 95%, generate one request until the HW valve position is less than 85%.
- Else if the HW valve position is less than 95%, do not generate requests.

For the SAT reset, the upper bound of the setpoint is determined using a linear function based on the outdoor air temperature, as shown in Figure 2. The CW reset adjusts both the CW temperature setpoint and CW differential pressure (DP) setpoint. When requests generate, the CW reset first increases the CW DP setpoint and does not adjust the CW temperature setpoint until the CW DP setpoint reaches its maximum value.

Algorithm 1: Trim & respond logic

Data: number of requests: N,
number of ignored requests: N_{ignore},
upper and lower bounds of setpoint: SP^{max} and SP^{min},
default value of setpoint: SP^0,
trim: SP^-,
respond: SP^+,
upper bound of respond: SP^+_{max},
Result: setpoint: SP

1 initialization, $SP = SP^0$;
2 if $N \leq N_{ignore}$ then
3 | $SP = \max(SP - SP^-, SP^{min})$;
4 else
5 | $SP = \min(SP + \min((N - N_{ignore})SP^+, SP^+_{max}), SP^{max})$;
6 end

Table 1.: Control sequences from ASHRAE Guideline 36

| Name	Control Logic	Inputs	Outputs
Duct static pressure reset	Trim & respond logic	Zone airflows and damper positions	Static pressure setpoint
Supply air temperature (SAT) reset	Trim & respond logic	Zone temperatures and cooling signals	SAT setpoint
Chilled water (CW) reset	Trim & respond logic	SAT and cooling coil valve positions	CW temperature setpoint and CW differential pressure (DP) setpoint
Hot water (HW) reset	Trim & respond Logic	SAT and HW coil valve positions	HW temperature setpoint
Demand controlled ventilation (DCV)	Proportional control	Indoor CO_2 concentration	Zone minimum airflow setpoint and air handling unit (AHU) minimum outdoor airflow setpoint
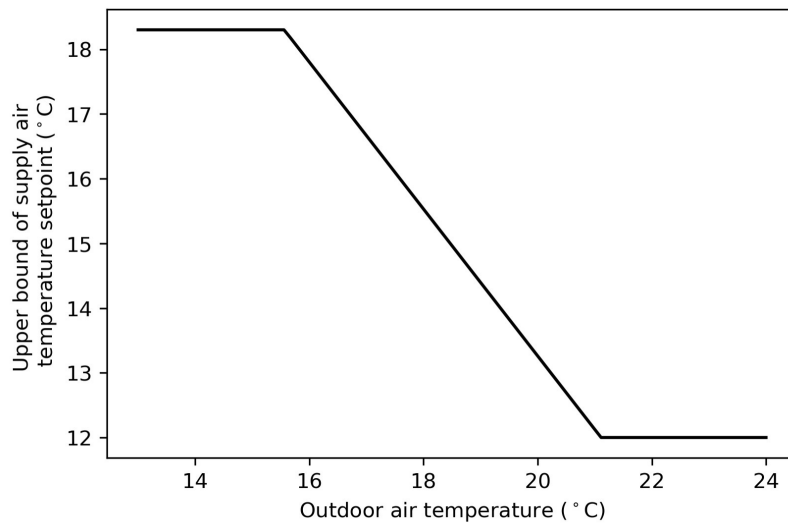
Figure 2.: The upper bound of the SAT setpoint.

The DCV utilizes a proportional control, as described in Equation 1, to adjust the minimum airflow setpoint:

$$V_m = V_m^- + (V_m^+ - V_m^-) \cdot \zeta, \tag{1}$$

where V_m is the minimum zonal airflow setpoint, V_m^+ and V_m^- are the lower bound and the higher bound of V_m, respectively, and ζ is the CO_2 control signal (0-1), which is calculated by

$$\zeta = \max(\min(\frac{c_{CO_2} - 700}{200}, 1), 0), \tag{2}$$

where c_{CO_2} is the indoor CO_2 concentration (ppm). The zone population-based minimum outdoor airflow setpoint is also reset from zero to its maximum value similarly based on ζ. The AHU minimum outdoor airflow setpoint is then re-calculated based on the new setpoints according to ASHRAE Standard 62.1 [32].

3.1.2. Control Verification

Algorithm 1, Equation 1, and Equation 2 are implemented in Python(version 3.10). To ensure the desired control output, a thoughtful validation of all the control sequences is also performed. This validation is an open-loop test in which the inputs for the control sequences are prescribed. Accordingly, the desired outputs of the control sequences are generated based on the interpretation of those sequences and compared to the test output. As an example, Figure 3 illustrates the inputs and outputs of the validation for the duct static pressure reset. One can see that the test output is identical to the expected values of this validation. More validation results can be found in Appendix A.
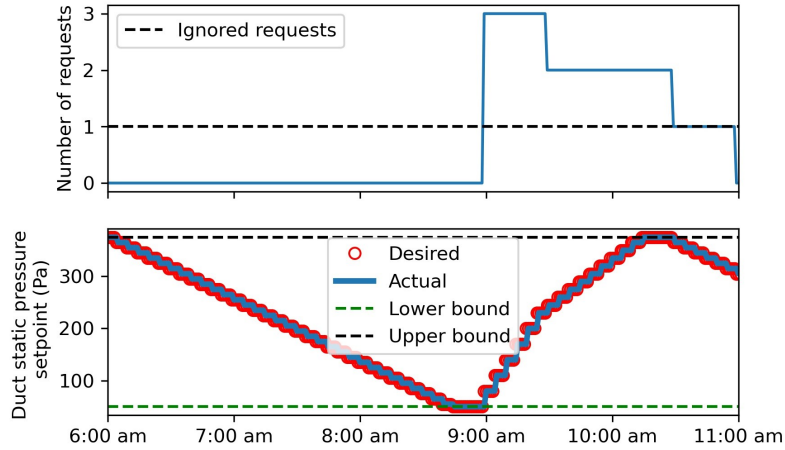

Figure 3.: Duct static pressure reset verification.

3.2. Building Model Development

3.2.1. System Description

This study considers a VAV system that serves a single floor of a typical medium ofice building located in Chicago, IL (cold and humid climate). This medium ofice building is defined based on the DOE commercial reference buildings [33]. Specifically, this floor has five zones: a core zone with floor area of 985 m^2, north and south zones with floor areas of 208 m^2 each, and east and west zones with floor areas of 131 m^2 each.

As illustrated in Figure 4, this VAV system consists of six subsystems:

- AHU. The AHU processes the supply air. It has a heating coil, a cooling coil, a supply fan, and a minimum eficiency reporting value (MERV) 13 filter [34]. There are valves that are connected with the heating coil and the cooling coil, respectively. Those valves, the CW valve and the HW valve, are controlled by local controllers to maintain the SAT based on its setpoint. The speed of the supply fan is controlled based on the duct static pressure setpoint.
- Terminal. The terminal adjusts the amount of air supplied to the zones and reheats the supply air under heating conditions. It consists of a damper and a heating coil, which are both controlled based on the zone temperature setpoint. The damper position is also subject to the minimum airflow setpoint.
- Chiller plant. The chiller plant provides cooling energy to the AHU. It is composed of a chiller and a CW pump. The chiller and the CW pump are controlled based on the CW temperature setpoint and the CW DP setpoint, respectively.
- Hot water plant. The HW plant provides heating energy to the AHU and the terminals. It consists of a heat pump and HW pump. The heat pump is controlled based on the HW temperature setpoint and the HW pump is controlled based on a constant DP setpoint.
- Zone. The zone represents the indoor environment, in which heat gains from the internal activities are absorbed by the indoor air and occupants exhale CO_2 and virus. In addition, the indoor environment also exchanges heat with the ambient environment.
- Duct network. The duct network distributes the supply air to each zone and mixes the return air with the fresh outdoor air. The outdoor air damper, the exhaust damper, and the recirculation damper are coupled and controlled to meet the AHU minimum outdoor airflow setpoint and provide economizing.
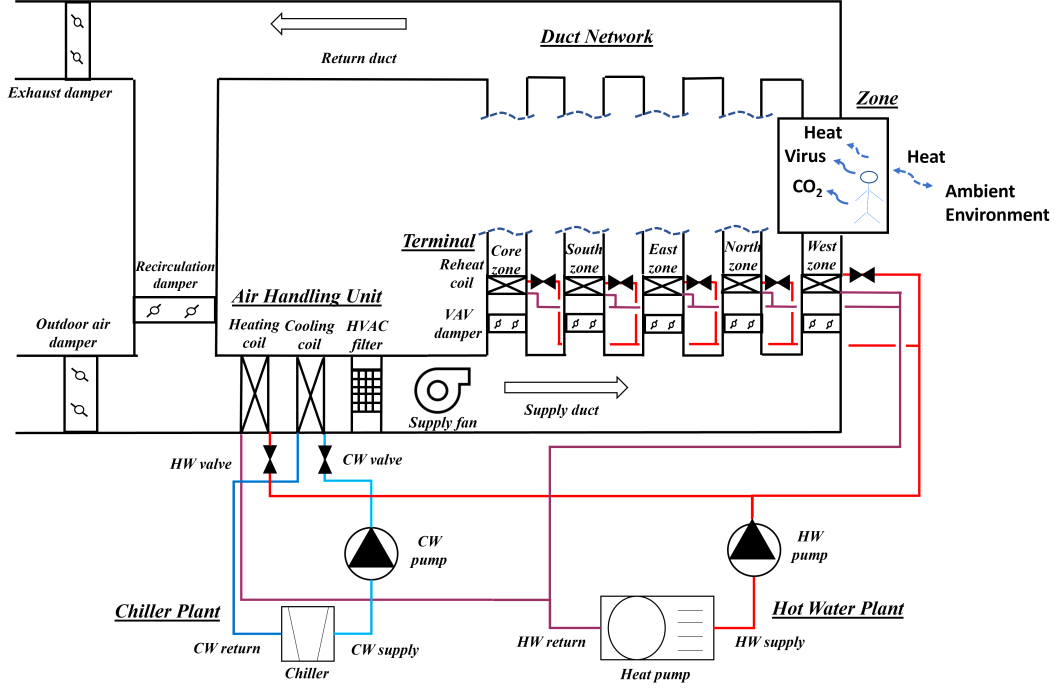
Figure 4.: Schematic of the studied variable air volume system.

3.2.2. System Modeling

When developing the system model of the studied system, this work leveraged a high-fidelity model of this building system from the IBPSA Project 1 BOPTEST library [12]. The model covers all the subsystems of the studied system. However, it does not consider the MERV 13 filtration in the AHU and the virus generated from the occupants. To support the comprehensive evaluation of G36, two Modelica component models were implemented to represent the MERV 13 filter and the generation and decay of virus in the zones based on a schedule of sick people, respectively. In what follows, the MERV 13 filter and indoor virus models are introduced.

First, the pressure drop imposed by the filter on the airflow and removal of the viral particles from the airflow is included in this model. The MERV 13 filter model in this study has a nominal pressure drop of 187 Pa based on the nominal flow rate and available data [35]. Note that the simulated pressure drop varies quadratically based on the flow rate and nominal settings as described in [36]. The MERV 13 filter model also simulates the removal of viral particles from the airflow based on a defined eficiency:

$$c_{out} = (1 - \eta_{filter})c_{in}, \qquad (3)$$

where c_{out} is the virus concentration exiting the filter, η_{filter} is the filter removal eficiency in terms of percentage of virus removed, and c_{in} is the virus concentration entering the filter. The filter eficiency can be between 0-100%, where $\eta_{filter} = 100\%$ describes a filter that completely removes all viral particles from the airflow. The virus removal eficiency of the modeled MERV 13 filter is 85% in this paper based on ASHRAE technical resources [37] and assuming viral particles with diameters of 1-3

10

µm. Various levels of MERV filtration can be studied using this model to compare impacts on IAQ and energy for indoor virus scenarios, as shown in [36, 38]. In this study, only MERV 13 filtration is studied for simplicity.

The virus concentration in each zone is calculated based on a mass balance:

$$\frac{dc_{zone}}{dt} = (1/m_{air,zone})[\Sigma(\dot{m}c)_{in} - \Sigma(\dot{m}c)_{out}] + \dot{c}_{gen,zone} - \dot{c}_{decay,zone}, \qquad (4)$$

where $\frac{dc_{zone}}{dt}$ is the rate of change of virus concentration in the zone with respect to time, $m_{air,zone}$ is the mass of air in the zone, $\Sigma(\dot{m}c)_{in}$ is the sum of the virus concentration flowrates into the zone, $\Sigma(\dot{m}c)_{out}$ is the sum of the virus concentration flowrates out of the zone, $\dot{c}_{gen,zone}$ is the virus concentration generation rate within the zone, and $\dot{c}_{decay,zone}$ is the rate of viral decay in the zone, which is modeled based on a first order method:

$$\dot{c}_{decay,zone} = k_{decay}c_{zone}, \qquad (5)$$

where k_{decay} is a defined constant rate of viral decay, and c_{zone} is the virus concentration in the zone. It is assumed that one sick person is present in each zone working a typical 9:00 AM to 5:00 PM Monday-Friday schedule throughout the year. This allows for analysis of the IAQ during different control scenarios throughout the year. The sick people generate viral particles into the well-mixed zones at a typical constant rate of 25 quanta/hr [39, 40], where a quantum is the viral dose expected to cause an infection in 63% of susceptible people. Thus, $c_{gen,zone}$ in Equation 4 is treated as a constant source term, during the defined working schedule, of 25 quanta/hr. A typical constant rate of decay of 0.48 hr^{-1} based on the literature [41] is adopted in this work. The outdoor air is assumed to have zero virus concentration. More about the Modelica implementation of the filter and virus transmission models can be found in [36].

In addition, occupants also generate CO_2 in the zones based on a constant generation rate of 0.0048 L/s per person [42]. The CO_2 concentration in each zone is calculated similar to Equation 4, except decay of CO_2 is not modeled. The outdoor air is assumed to have a CO_2 concentration of 400 ppm [42].

3.3. Control Evaluation

3.3.1. Metric Definition

To facilitate the control evaluation, this work considers the following evaluation metrics. The first metric is the energy consumption, including energy consumption of the fan, cooling energy from the chiller and CW pumps, and heating energy from the heat pump and HW pumps. Since all the devices are powered by electricity, they can be fairly compared to one another based on their energy consumption.

The second metric is virus concentration. Specifically, the average virus concentrations during typical work hours: 9:00 AM to 5:00 PM Monday through Friday throughout the year is calculated. This is also identical to the schedule of sick people generating viral particles. These averages are computed as the building average using a weighted sum of the five zones of this floor.

The third metric is the risk of infection. The predicted number of infections in the

building using the Wells-Riley approach [43] is calculated. The risk of infection is based on the amount of viral particles inhaled by occupants over time:

$$R(t) = 1 - \exp(-IR \int_{t_0}^{t} c(t)\, dt), \tag{6}$$

where $R(t)$ is the risk of infection over time, t, since initial time, t_0, IR is the inhalation rate, and $c(t)$ is the virus concentration over time. The predicted number of infections is then based on the calculated risk multiplied by the number of occupants in the zone. To account for the dynamic occupancy schedules in the zone, the predicted number of infections during time intervals when the occupancy is constant is calculated. The predicted number is then added to the accumulated predicted number of infections in the previous time interval to build the dynamic accumulated predicted number of infections:

$$R_{0,T}(t) = S_T \left[1 - \exp(-IR \int_{t_0}^{t} c(t)\, dt)\right] + R_{0,T-1}(t_0), \tag{7}$$

where $R_{0,T}(t)$ is the dynamic predicted number of infections during time interval, T, and S_T is the number of susceptible occupants in this interval. The total predicted number of infections can be determined based on the sum of predicted infections in each zone.

The fourth metric is thermal discomfort, which is computed as the integral of the deviation from the setpoint during occupied hours, averaged among the zones, given by:

$$T_{dis} = \frac{\Sigma_{zone=1}^{n} \int [\max(T_{zone} - T_{coo,set}, 0) + \max(T_{hea,set} - T_{zone}, 0)]dt}{n}, \tag{8}$$

where T_{dis} is the thermal discomfort, n is the number of zones, T_{zone} is the zone temperature, $T_{coo,set}$ is the cooling setpoint temperature, and $T_{hea,set}$ is the heating setpoint temperature. The cooling and heating setpoints during occupied hours are 24 $^\circ$C and 21 $^\circ$C, respectively.

The final metric is CO_2 discomfort, which is calculated similarly as:

$$CO_{2dis} = \frac{\Sigma_{zone=1}^{n} \int [\max(c_{CO_2,zone} - c_{CO_2,set}, 0)]dt}{n}, \tag{9}$$

where CO_{2dis} is the CO_2 discomfort, $c_{CO_2,zone}$ is the zone CO_2 concentration, and $c_{CO_2,set}$ is the CO_2 setpoint, which is 900 ppm in this study. The max functions in these equations are used to count only the unwanted deviations from the setpoints and otherwise set the discomfort to zero. This includes deviations above the cooling or CO_2 setpoints and deviations below the heating setpoint.

3.3.2. Co-simulation Setup

To perform the control evaluation, this work set up a co-simulation between the Python-based implementation of G36 and the system model. As illustrated in Fig-ure 5, this co-simulation setup leverages the BOPTEST Framework to simulate the system model. In addition, this co-simulation setup realizes a loose coupling between G36 and the system model, i.e., G36 and the system model are not executed simultaneously but sequentially. Specifically, G36 initializes itself and the system model at the beginning of the co-simulation, then G36 pauses the execution. Once the system model completes the initialization (simulation time equals to t_0), it then triggers G36 to resume the execution and pauses the simulation. When G36 completes one-step execution, it triggers the simulation to resume and pauses the execution. The simulation advances until it reaches $t_0 + \delta t$, then pauses and triggers G36 to resume the execution. The previous steps continue until the simulation reaches the end time. Note that this work set $\Delta t = 5$min. In addition, the parameters of G36 are set based on Table 2.
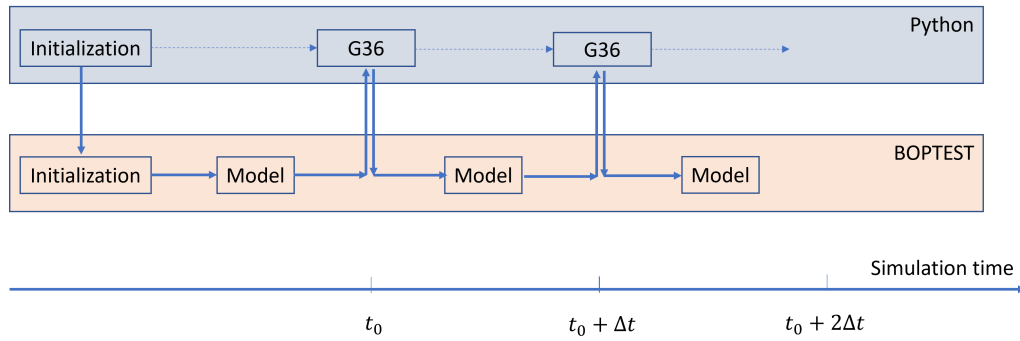

Figure 5.: Co-simulation setup for the control evaluation

Table 2.: Parameters of G36

Name	Lower Bound	Upper Bound	Default	Trim	Respond	Maximum Respond
Duct static pressure reset	50 Pa	375 Pa	375 Pa	-10 Pa	15 Pa	37 Pa
SAT reset	12°C	18.3°C	12°C	0.1°C	-0.2°C	-0.6°C
CW reset (temperature)	6°C	10°C	6°C	2%	-3%	-7%
CW reset (DP)	30 kPa	45 kPa	45 kPa	-2%	3%	7%
HW reset	32.2°C	71.1°C	71.1°C	-1.11°C	1.67°C	3.89°C

4.   Results and Discussions

This section first provides the general results for the baseline and G36. Detailed analysis is then included to examine the controls for a typical heating day and cooling

day. Based on these results, the DCV is modified to be less aggressive to alleviate the significant increase in energy consumption. Finally, the results and limitations are discussed.

4.1. General Results

Table 3 summarizes the results for the baseline and G36. One can see that G36 reduces the annual energy consumption by about 11% compared to the baseline control. While the thermal discomfort shows a small increase of about 5% for G36, the DCV completely eliminates the CO_2 discomfort from the baseline. The average virus concentration also decreases by 13% for G36 because of the DCV.

Table 3.: Summary of results.

Control	Annual Energy Consumption (MWh)	Thermal Discomfort ($^\circ$C $\cdot$ hr)	CO_2 Discomfort (ppm $\cdot$ hr)	Average Virus Concentration (quanta/m^3)
Baseline	62.4	210	1636	8.2×10^{-3}
G36	55.4	221	0	7.1×10^{-3}

Figure 6 shows the breakdown of annual energy consumption. The majority of energy savings from G36 comes from a 43% decrease in heating energy. There is also a 28% increase in fan energy with G36 and almost no change in cooling energy. The decrease in heating energy appears to be a result of the SAT and HW reset. The increase in fan energy is a result of the DCV.
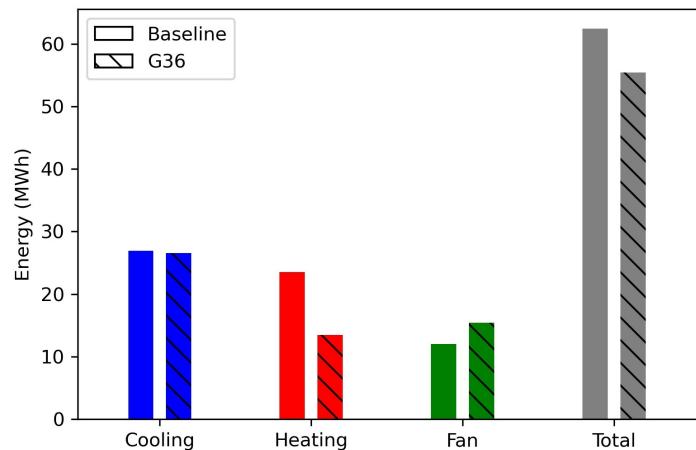

Figure 6.: Breakdown of annual energy comparison for baseline and G36 cases.

Figure 7 shows the dynamic air-side setpoints throughout the year using G36. The static pressure setpoint decreases toward its minimum in the morning, but often increases toward its maximum in the afternoon. The increase in the afternoon is due to

the DCV, which increases the minimum airflow to the zones when the CO_2 concentration is high. This increase in the afternoon does not happen as frequently during the shoulder seasons because of lower CO_2 concentrations as more outdoor air is used for economizing during these seasons. The SAT setpoint increases toward its maximum value during the cooler months of the year when not much cooling is needed. During the warmer months in the middle of the year, the SAT tends to remain at its minimum value to provide enough cooling to the zones. It is also constrained based on the warmer outdoor conditions during this time.

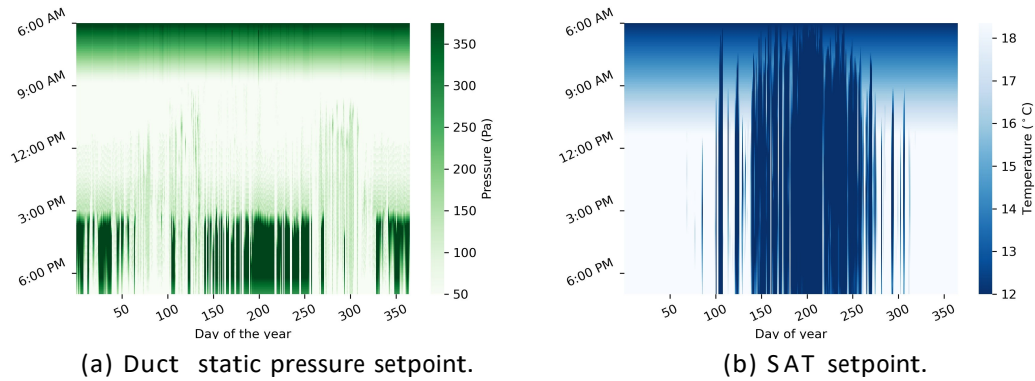(a) Duct static pressure setpoint.   (b) SAT setpoint.

Figure 7.: Dynamic air-side setpoints throughout the year using G36.

Figure 8 shows the dynamic water-side setpoints with G36. The CW temperature and CW DP setpoints tend to decrease toward the maximum temperature and minimum differential pressure during the cooler months of the year and trend toward the minimum temperature and maximum differential pressure during the summer months. This is because the CW needs to be cooler and more flow is required in the warmer months to provide cooling. While the cooling demand is typically highest on summer afternoons, there are a few very hot days in the middle of the year, when the cooling demand is also very high in the morning and the CW temperature setpoint tends toward its minimum. There are also some exceptions where these setpoints periodically increase during the cooler months. This is a result of other changing setpoints, such as the SAT setpoint. CW requests are generated when the SAT exceeds its setpoint by a defined threshold, which happens for short periods during the cooler months as the air-side setpoints change and the system needs time to respond to the dynamic setpoints. Lastly, the HW temperature setpoint increases during the mornings in the coolest times of the year, when more heating is required. Otherwise, it often decreases toward its minimum value.

15

(a) CW temperature setpoint.
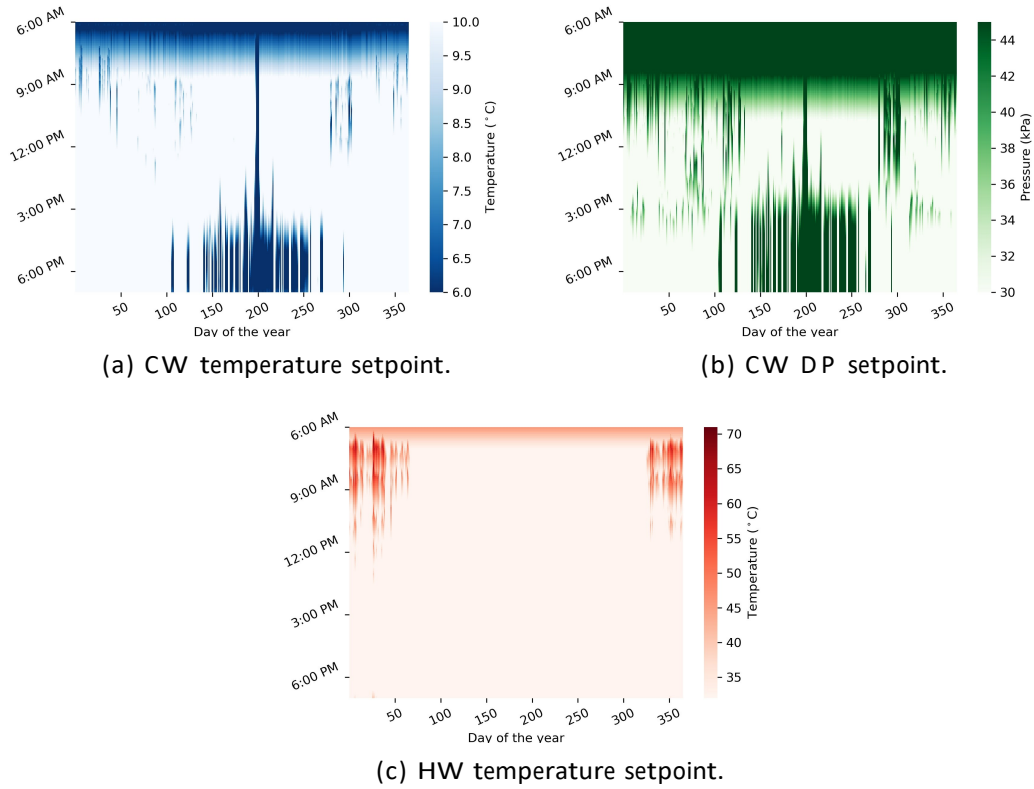

(b) CW DP setpoint.

(c) HW temperature setpoint.

Figure 8.: Dynamic water-side setpoints throughout the year using G36.

Figure 9 shows the average building temperatures throughout the year for the baseline and G36. The average temperature for the baseline is straightforward: it is around the heating setpoint of 21 °C during the cooler months and around the cooling setpoint of 24 °C during the warmer months. However, the building appears to be overcooled during some summer afternoons with G36. This is a result of the DCV, which tends to increase airflow to the zones in the afternoon, when the CO_2 concentration is high. During the cooler months, the SAT can be increased to prevent overcooling. However, the maximum SAT is constrained based on the outdoor air temperature for G36. Thus, even though the zones are overcooled, the SAT cannot be increased because the outdoor air temperature is too high during the warmer months.
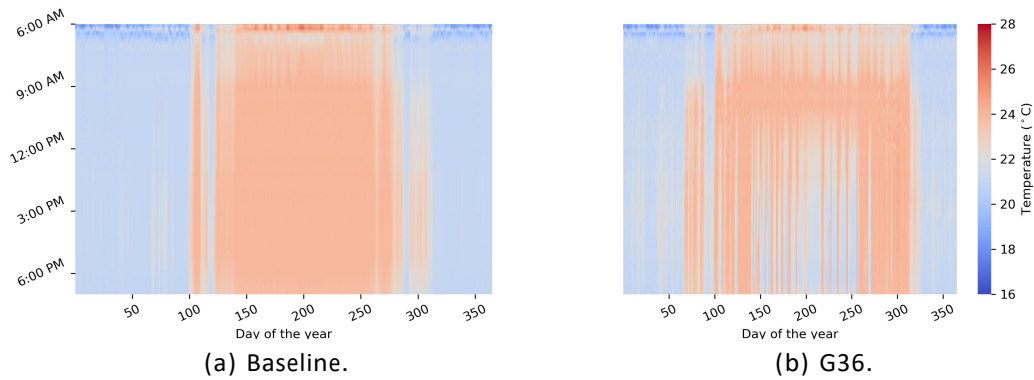

(a) Baseline.

(b) G36.

Figure 9.: Average building temperature throughout the year for the baseline and G36.

16

Figure 10 shows the dynamic CO_2 and virus concentrations for the baseline and G36. For both cases, the CO_2 concentration initially decreases as the HVAC system turns on around 6:00 AM, then begins to increase around 9:00 AM as more occupants arrive. In the baseline case, the CO_2 concentrations are lower during the shoulder seasons, when more outdoor air is used for economizing. They are comparatively higher in the winter and summer months, when the HVAC system tends to supply the minimum outdoor air. For G36, the decrease in CO_2 concentration during the shoulder seasons is less significant. This is because the increase in SAT due to G36 can reduce the amount of outdoor air used for economizing compared to the baseline. Additionally, the CO_2 concentration for G36 often decreases in the afternoon after reaching a peak. This is a result of the DCV, which increases ventilation to the zones when the CO_2 concentration becomes high in the afternoon.

For both cases, the virus concentrations begin to increase around 9:00 AM, when the sick people arrive, then decrease after 5:00 PM, when the sick people leave. The effect of outdoor air on the virus concentration is less significant compared to the CO_2 concentration, as shown by higher virus concentrations in the shoulder seasons. This is because the MERV 13 filter is able to remove 85% of the viral particles in the supply airflow, so diluting the supply airflow with more outdoor air is relatively less impactful. Instead, the supply airflow rate is more impactful, since this determines the rate of virus removal at the filter as well as the ventilation rate to the zones. Because of this, the virus concentration is higher in the shoulder seasons, when the supply airflow rate is lower, and is also lower during the summer, when the airflow rate is higher. The virus concentration for the G36 case is driven by the DCV, since this impacts the overall supply airflow rate and the zone ventilation rates. The virus concentration peaks earlier in the day, then decreases in the afternoon as the DCV increases ventilation due to the high CO_2 concentration. The virus concentration is sometimes higher in the shoulder seasons, when the CO_2 concentration is lower, since the DCV does not increase the ventilation as much.

(a) CO_2 concentration (baseline).

(b) CO_2 concentration (G36).

(c) Virus concentration (baseline).

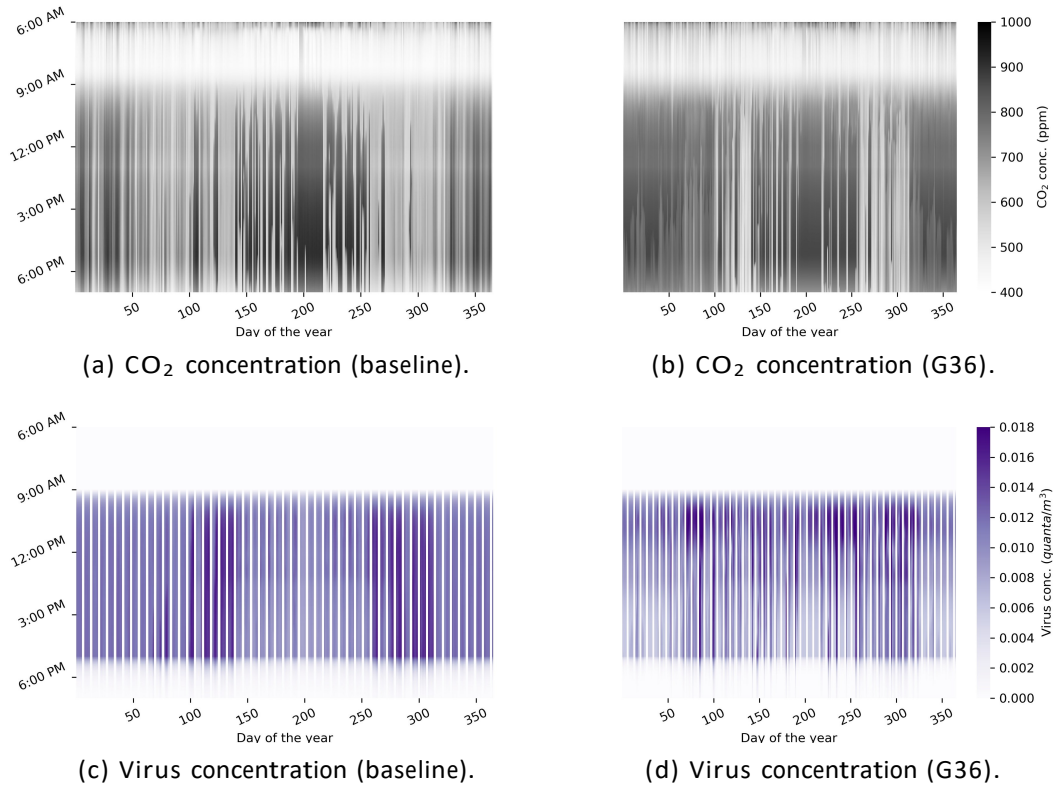(d) Virus concentration (G36).

Figure 10.: Dynamic concentrations throughout the year for the baseline and G36.

4.2. Detailed Analysis

This section provides detailed analyses of the baseline and G36 controls. The control performances are shown first for a typical heating day, then a typical cooling day.

4.2.1. Typical Heating Day

The combination of the HW and SAT resets for a typical heating day leads to heating energy savings for G36. First, Figure 11 shows the HW temperature setpoint/temperature and the HW valve positions for the baseline and G36. The HW temperature setpoint increases for G36 in the morning as the reheat valves open past the threshold of 95%, particularly for the North and East zones. There are some oscillations in the HW valve positions for the G36 case in the morning because of the changing control setpoint. Eventually, the reheat valves begin to close and the HW temperature setpoint decreases toward its minimum. This leads to 54% heat pump energy savings for G36 on this day.
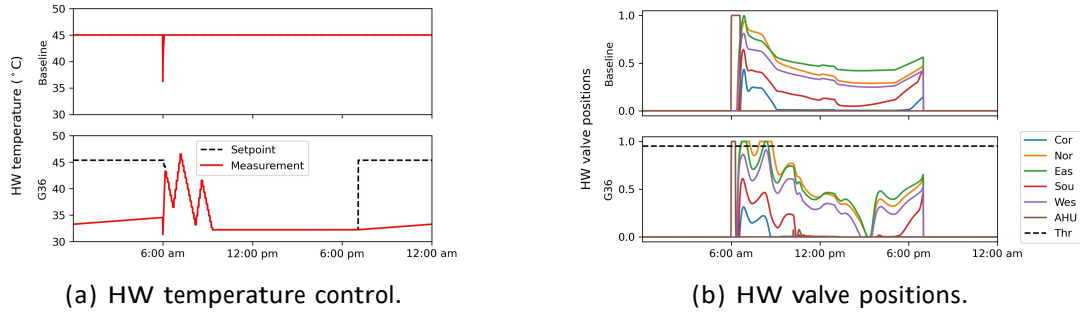
(a) HW temperature control.

(b) HW valve positions.

Figure 11.: HW control and HW valve positions for a typical heating day.

Figure 12 shows the SAT control for this day as well as the outdoor air usage. The SAT increases for G36 since cooling is not required for this winter day. It also appears that the system sometimes requires more time to respond to the changing setpoint, shown by the deviation between the measured SAT and setpoint around 10:00 AM and 3:00 PM. This is partially a result of other changing setpoints, such as the duct static pressure and minimum outdoor airflow setpoints. These changing setpoints can also lead to oscillations in the SAT and outdoor airflow for the G36 case, for example around 12:00 PM. Neither case uses CW cooling at the AHU on this cold day, but rather more outdoor air is used for economizing in the baseline case because of the lower SAT. The higher SAT with G36 saves heating energy since less heating is required at the reheat coils for the zones, but the reduction in outdoor air impacts the IAQ on this day. The deviation of the measured outdoor airflow from the minimum setpoint impacts the SAT for G36.
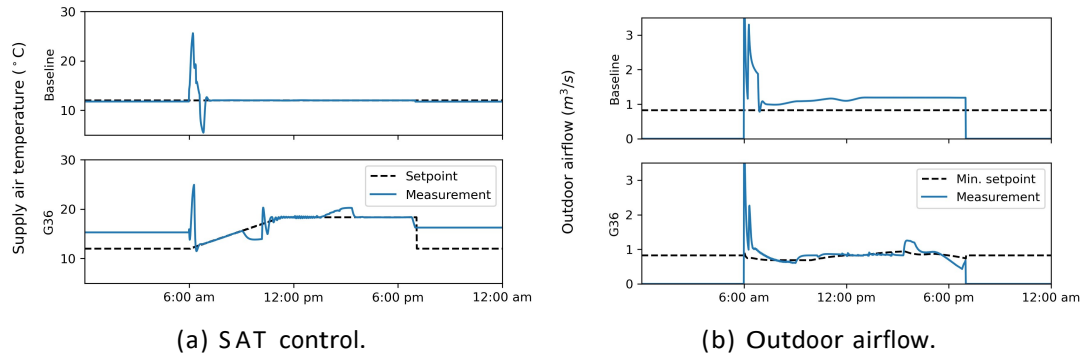

(a) SAT control.

(b) Outdoor airflow.

Figure 12.: SAT and outdoor airflow control for a typical heating day.

Figure 13 shows the IAQ metrics for this heating day. The CO_2 concentrations in the zones are lower for the baseline case because of the higher outdoor air usage. Despite this, the virus concentrations in the zones and total predicted number of infections in the building are lower for the G36 case. This is because the virus concentration is more sensitive to the total airflow rate rather than outdoor airflow rate. The total airflow rate is higher in the afternoon for the G36 case because of the DCV, which increases the ventilation to the zones when the CO_2 concentration surpasses the reset threshold of 700 ppm. As a result, the predicted number of infections decreases from 3.1 with the baseline control to 2.3 for G36. For the baseline control, this is interpreted as three infections are predicted with a 10% chance of a fourth one occurring, and for G36 two infections are predicted with a 30% chance of a third occurring.

(a) CO_2 concentration.

(b) Virus concentration.
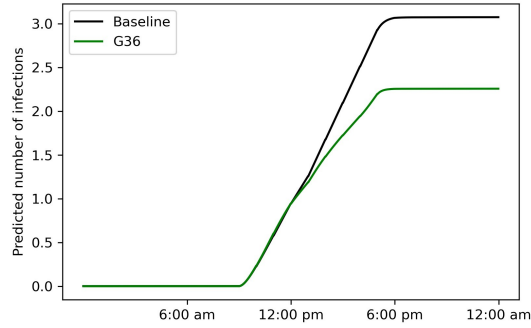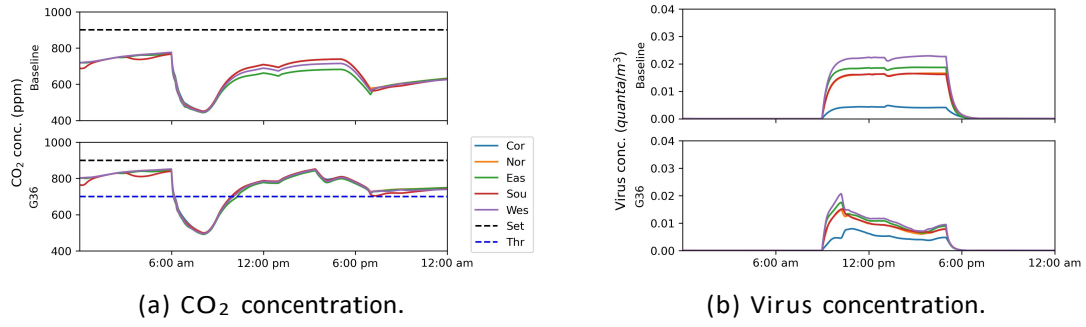

(c) Total predicted number of infections.

Figure 13.: IAQ metrics for a typical heating day.

Figure 14 shows the zone airflows, damper positions, and the duct static pressure for the typical heating day. While the zone airflows tend to be constant at their heating setpoint for the baseline case, they are dynamic with G36. The shape of the increase in the zone airflows is consistent with the pattern of the zone CO_2 concentrations, since this drives the increase in airflow via the DCV.

The zone airflows (most noticeably the Core zone) oscillate some due to the changing zone setpoints and AHU setpoints caused by the G36 control during this period. This is further demonstrated by the significant oscillations in the damper positions during the afternoon for G36. The oscillations of the dampers above and below the threshold to generate requests leads to oscillations in the duct static pressure setpoint as well.

Note that similar oscillations are not observed in the results of the baseline case. This suggests that G36 may pose significant challenges to the operation of the local feedback control loops.
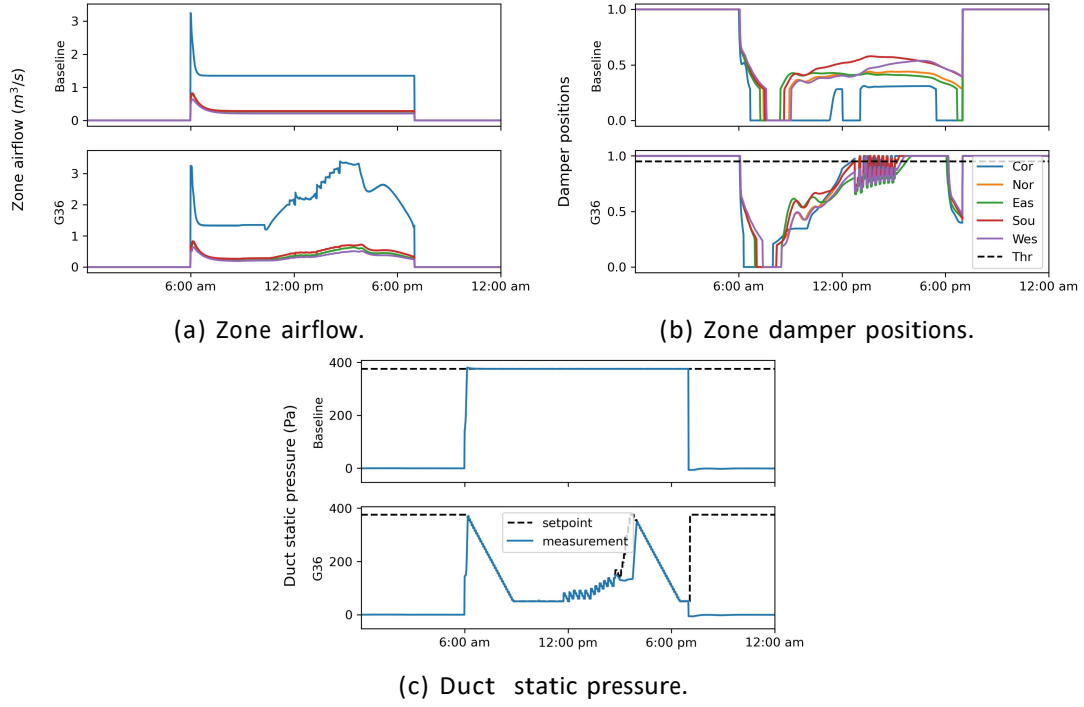
(a) Zone airflow.

(b) Zone damper positions.

(c) Duct static pressure.

Figure 14.: Zone airflow, damper positions, and duct static pressure for a typical heating day.

4.2.2. Typical Cooling Day

Next, results for a typical cooling day are shown to demonstrate the differences in the controls for this day. Figure 15 shows the IAQ metrics for this typical cooling day. Unlike the heating day, the CO_2 concentration is higher for the baseline case on this day. This is because the baseline control supplies the minimum outdoor airflow on this hot day, so the CO_2 concentration increases faster. The CO_2 concentration for G36 remains below the setpoint because of the DCV, which behaves similarly as previously shown for the heating day. The virus concentration is also lower with G36 because of the DCV, although it is less significantly lower than the baseline on this day compared to the heating day. This is because the airflow to the zones for the baseline control is higher on this cooling day compared to the heating day.
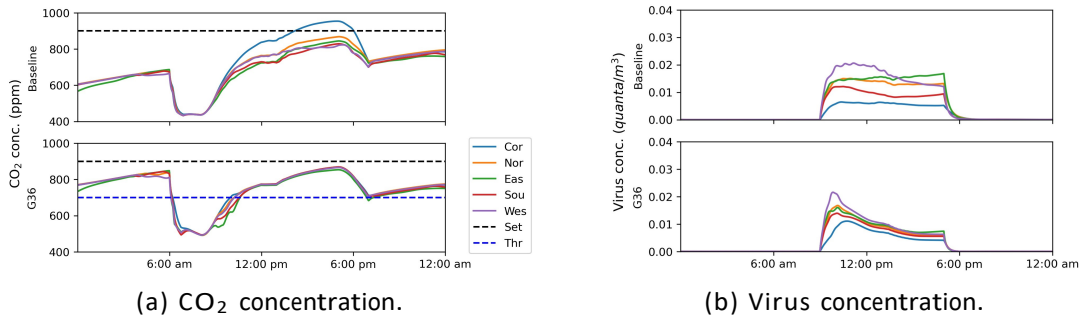

(a) CO_2 concentration.

(b) Virus concentration.

Figure 15.: IAQ metrics for a typical cooling day.

The DCV also negatively impacts the energy consumption. Figure 16 shows the

21

chiller and fan power and corresponding energy consumptions for this day. As the DCV increases ventilation to the zones in the afternoon, the fan power ramps up to increase the airflow and operates at its maximum speed for several hours. The fan power oscillates some during the ramping period because of the control-related oscillations of the duct static pressure setpoint, shown previously in Figure 14. The increase in airflow also impacts the CW return temperature, which leads to an increase in chiller power in the afternoon as well. Despite energy savings earlier in the day due to the other controls, the DCV ultimately leads to a significant increase in fan energy and small increase in chiller energy.
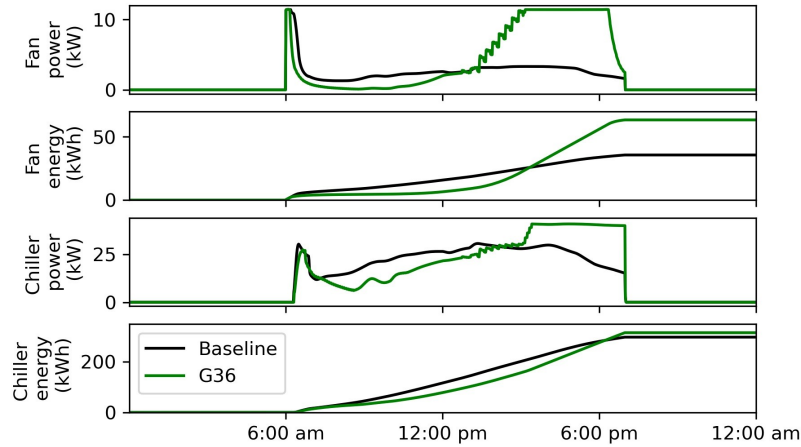

Figure 16.: Fan and chiller power for a typical cooling day.

4.3. Modified DCV

To study the interactions between the DCV and other G36 control sequences, G36 is tested with a small change to the DCV. Figure 16 shows the DCV helped reduce the virus concentration and maintain CO_2 levels, but lead to a significant increase in fan energy. To alleviate the large fan energy increase, the CO_2 threshold in the zones to begin the DCV is increased from 700 ppm to 800 ppm to make the DCV less aggressive. Table 4 summarizes the results with the updated G36 with increased the CO_2 threshold. The change in the control reduces the total energy consumption by 14% compared to the default G36. This includes a 46% reduction in fan energy and a 10% reduction in cooling energy as a result of the less aggressive DCV. There is also a small (3%) increase in thermal discomfort compared to G36 with default settings.

Table 4.: Summary of modified G36 results.

Control	Annual Energy Consumption (MWh)	Thermal Discomfort ($^{\circ}$C $\cdot$ hr)	CO_2 Discomfort (ppm $\cdot$ hr)	Average Virus Concentration (quanta/m^3)
Baseline	62.4	210	1636	8.2×10^{-3}
G36	55.4	221	0	7.1×10^{-3}
Modified G36	47.7	238	0	8.5×10^{-3}

22

Interestingly, the change to the DCV does not impact the CO_2 discomfort, but more significantly impacts the virus concentration. This is because the modified DCV is able to still maintain the CO_2 concentration below the setpoint. However, the supply airflow throughout the day decreases with the modified DCV, which reduces the rate at which the virus is filtered from the supply airflow and ventilated from the zones. This leads to virus concentration levels similar to the baseline, which does not use DCV. These results demonstrate the tradeoffs of energy eficiency and IAQ for advanced control strategies. Furthermore, the results show the potential to improve the system performance by tuning the G36 parameters.

4.4. Discussion

To sum up, G36 impacts both energy consumption and IAQ. Heating energy can be saved with G36 via the SAT and HW reset. However, the heating energy is saved in large part because of a decrease in outdoor air used for economizing. Thus, the CO_2 concentration with G36 increases during these scenarios due to less outdoor air usage. G36 can increase the fan energy consumption due to the DCV, because the minimum airflow setpoints increase when the CO_2 concentration is low. The increase in airflow is beneficial to reducing the virus concentration, since this increases both the rate at which virus is filtered in the AHU and the ventilation to the zones. For cooling scenarios, the DCV maintains the CO_2 concentration below the setpoint in contrast to the baseline, which shows higher CO_2 concentrations when less outdoor air is used. However, the increased airflow caused by the DCV also increases the chiller power. This is a result of higher CW return temperatures caused by the significant heat rejected to the CW from the increased airflow.

There are key factors that impact the performance of G36. First, the DCV significantly impacted both energy consumption and IAQ. Because of this, the DCV is modified to be less aggressive and found that this alleviated the increase in fan energy consumption. The CO_2 concentration could still be controlled below the setpoint value. However, the virus concentration increased since the airflow was decreased with the modified control. Other parameters can potentially be tuned depending on the system and climate. For example, the zones were overcooled during the summer afternoons when the SAT was at its minimum and the DCV increased the airflow to the zones. Despite being overcooled, the SAT remained at its minimum since the outdoor air temperature was above the threshold to reset the SAT. Loosening this threshold could lessen the overcooling in the zones, although this needs to be done carefully since the SAT needs to be low for dehumidification as well. Finally, the local feedback control loops may need to be re-tuned before implementing G36. For example, the damper positions also oscillated significantly with G36 and caused oscillations in the duct static pressure. To ensure control stability, it may be necessary to tune those local feedback control loops.

5. Conclusion

This work presented a simulation-based assessment of G36. More precisely, this work considers a typical medium ofice building in Chicago, IL. To represent the short-term dynamics of the studied building, a high-fidelity building energy model is implemented with Modelica. This building energy model is then co-simulated with G36, which is implemented in Python. Compared to existing works, this work provides a more com-

prehensive assessment of the overall performance of G36. It considers the interactions between different G36 control sequences. It also evaluates the impacts of G36 on long-term energy performance, short-term operation stability, and IAQ.

Based on the results, the following conclusions are drawn:

- G36 leads to a better building performance in terms of energy consumption and IAQ, but decreases the indoor thermal comfort level. The majority of energy savings from G36 are associated with the SAT and HW reset, which significantly reduces the heating energy consumption. Part of the heating energy savings is cancelled out by the increased energy consumption by fans. The decreases in both the CO_2 concentration and the average virus concentration are attributed to the DCV control. In the meanwhile, the thermal discomfort is slightly increased due to the reset logic.
- There is a trade-off between energy consumption and IAQ when using G36 control. To maintain the desired CO_2 concentration, G36 increases the ventilation to the zones, leading to higher energy consumption by the fan and the chiller in the summer. One can balance the trade-off between the energy consumption and IAQ to some extent, by adjusting the parameters in the DCV. The assessment results indicate that it is possible to further reduce the energy consumption un-der g36 without sacrificing the CO_2 comfort. However, this may lead to a higher virus concentration under virus scenarios.
- G36 poses the requirements of tuning the local feedback control. G36 impacts the operation of the local feedback control from two aspects. First, under G36, setpoints of local feedback control is time varying, even with oscillations. In this case, local feedback control needs to response fast in order to track the setpoint. Second, G36 changess setpoints of local feedback control simultaneously. Since local feedback control loops interact with each other, G36 essentially complicate the control process. Therefore, to unleash the potentials of G36, it is necessary to fine-tune the local feedback control.

Compared to existing works, there are limitations in this work. First, unlike the study performed by Pang et al. [17] where different climate zones are considered, this work only studies the weather in Chicago. The building energy model leveraged is designed for Chicago and changing it to accommodate other climate conditions require a sophisticated sizing process. In addition, this building energy model doesn't contain a detailed model for the building envelope but uses a lumped zone instead. This may affect the accuracy of simulation results in general. Since all the conclusions from this study is based on comparative results between G36 and baseline, we don't expect those limitations to affect the conclusions. There are some interesting directions for the future work. First, a more realistic building system model with explicit models for the condenser-side of the water systems can be used. The studied building model provides simplicity necessary to allow us to study G36 thoroughly. However, it doesn't explicitly model the condenser side of the chiller and heat pump, preventing the study of condenser water controls that are included in G36. Second, our study assumes a typical occupancy schedule and prescribed this schedule to repeat each week. However, actual occupancy and number of sick people is stochastic, so it would be beneficial to evaluate G36 under such stochastic conditions.
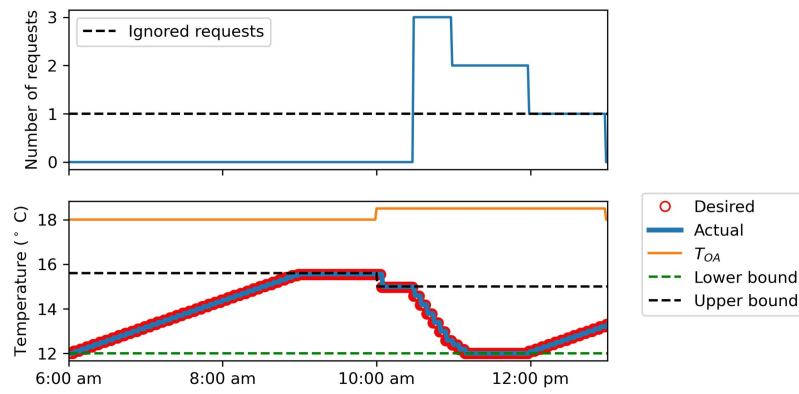
Appendix A: G36 Implementation Validation
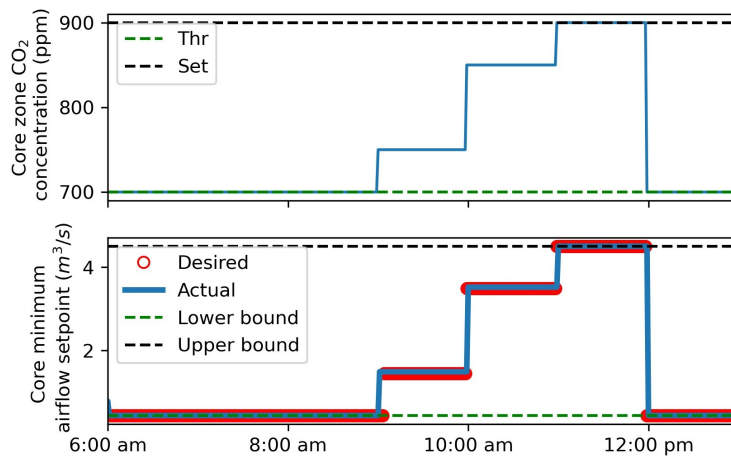

Figure A1.: SAT reset verification.
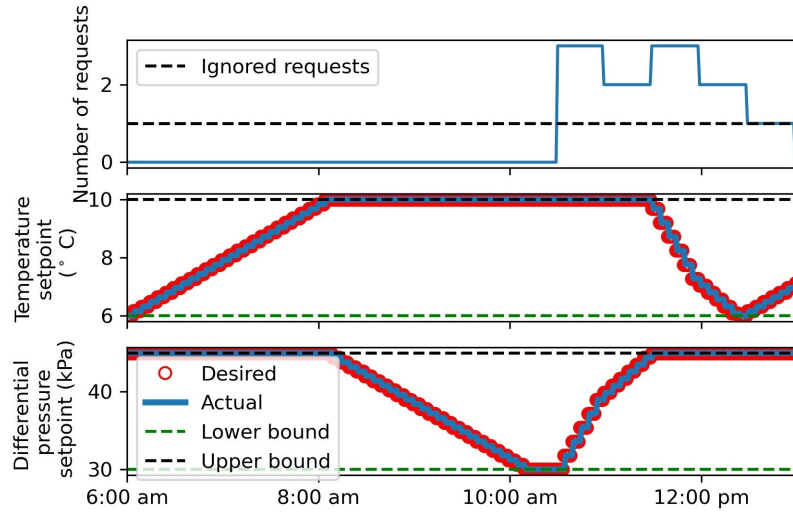

Figure A2.: DCV verification.
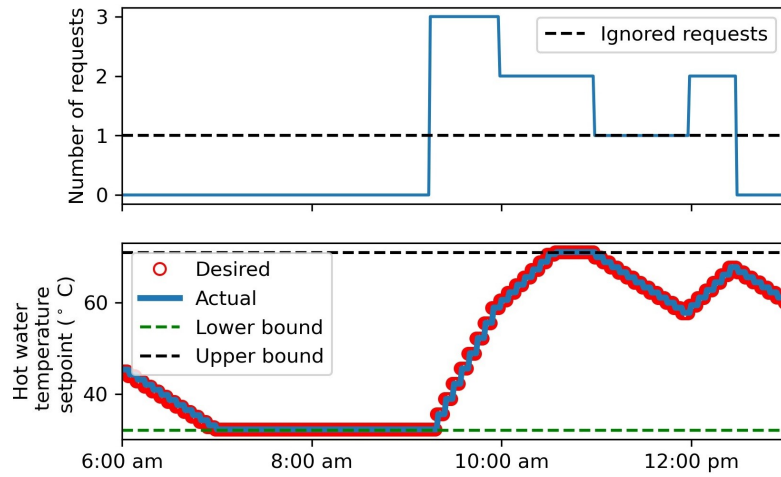
Figure A3.: CW reset verification.

Figure A4.: HW reset verification.

References

[1] S. Kiliccote, M. A. Piette, and D. Hansen, "Advanced controls and communications for demand response and energy eficiency in commercial buildings," 2006.

[2] M. Wetter, "A view on future building system modeling and simulation," in Building Performance Simulation for Design and Operation. Routledge, 2019, pp. 631–656.

[3] Z. J. Yu, F. Haghighat, and B. C. Fung, "Advances and challenges in building engineering and data mining applications for energy-eficient communities," Sustainable Cities and Society, vol. 25, pp. 33–38, 2016.

[4] G. H. Merabet, M. Essaaidi, M. B. Haddou, B. Qolomany, J. Qadir, M. Anan, A. Al-Fuqaha, M. R. Abid, and D. Benhaddou, "Intelligent building control sys-

tems for thermal comfort and energy-eficiency: A systematic review of artificial intelligence-assisted techniques," Renewable and Sustainable Energy Reviews, vol. 144, p. 110969, 2021.

[5] J. Drgoňa, J. Arroyo, I. C. Figueroa, D. Blum, K. Arendt, D. Kim, E. P. Ollé, J. Oravec, M. Wetter, D. L. Vrabie et al., "All you need to know about model predictive control for buildings," Annual Reviews in Control, 2020.

[6] ASHRAE, "ASHRAE Guideline36, High-Performance Sequences of Operation for HVAC Systems," 2021. [Online]. Available: https://www.ashrae.org/news/ashraejournal/guideline-36-2021-what-s-new-and-why-it-s-important

[7] M. Hydeman and B. Eubanks, "Advanced control sequences for HVAC systems-Phase I: air distribution and terminal systems," ASHRAE Research Project RP-1455 Final Report. Atlanta: ASHRAE, 2015.

[8] ASHRAE, "RP-1711 – Advanced Sequences of Operation for HVAC Systems – Phase II Central Plants and Hydronic Systems," 2014.

[9] J. Schein, S. T. Bushby, N. S. Castro, and J. M. House, "A rule-based fault detection method for air handling units," Energy and Buildings, vol. 38, no. 12, pp. 1485–1492, 2006.

[10] K. Zhang, D. H. Blum, M. Grahovac, J. Hu, J. Granderson, and M. Wetter, "Development and Verification of Control Sequences for Single-Zone Variable Air Volume System Based on ASHRAE Guideline 36," Lawrence Berkeley National Lab.(LBNL), Berkeley, CA (United States), Tech. Rep., 2020.

[11] S. E. Mattsson and H. Elmqvist, "Modelica-An international effort to design the next generation modeling language," IFAC Proceedings Volumes, vol. 30, no. 4, pp. 151–155, 1997.

[12] D. Blum, J. Arroyo, S. Huang, J. Drgoňa, F. Jorissen, H. T. Walnum, Y. Chen, K. Benne, D. Vrabie, M. Wetter et al., "Building optimization testing framework (BOPTEST) for simulation-based benchmarking of control strategies in buildings," Journal of Building Performance Simulation, vol. 14, no. 5, pp. 586–610, 2021.

[13] "Python," Python Releases for Windows, 2021.

[14] N. M. Ferretti, N. Milesi-Ferretti, M. A. Galler, S. T. Bushby, and J. Sorra, Commissioning ASHRAE High-Performance Sequences of Operation for Multiple-Zone Variable Air Volume Air Handling Units. US Department of Commerce, National Institute of Standards and Technology, 2019.

[15] N. Nassif, "Field and Simulation Testing and Improvement of ASHRAE Guideline 36 Duct Static Pressure Resetting Algorithm," ASHRAE Transactions, vol. 128, no. 1, 2022.

[16] Y. Yoon, Y. Li, P. Im, and Y. Bae, "Implementation of ASHRAE Guideline 36 Control Logic into Oak Ridge National Laboratory (ORNL)'s Flexible Research Platform (FRP)," Oak Ridge National Lab.(ORNL), Oak Ridge, TN (United States), Tech. Rep., 2022.

[17] Z. Pang, Y. Chen, J. Zhang, Z. O'Neill, H. Cheng, and B. Dong, "Nationwide HVAC energy-saving potential quantification for ofice buildings with occupant-centric controls in various climates," Applied Energy, vol. 279, p. 115727, 2020.

[18] ASHRAE, "Standard 90.1 Energy Eficiency Standard for Buildings Except Low-Rise Residential Buildings," American Society of Heating, Refrigerating and Air-Conditioning Engineers, 2019.

[19] D. B. Crawley, L. K. Lawrie, F. C. Winkelmann, W. F. Buhl, Y. J. Huang, C. O. Pedersen, R. K. Strand, R. J. Liesen, D. E. Fisher, M. J. Witte et al.,

"EnergyPlus: creating a new-generation building energy simulation program," Energy and Buildings, vol. 33, no. 4, pp. 319–331, 2001.

[20] M. Deru, K. Field, D. Studer, K. Benne, B. Grifith, P. Torcellini, B. Liu, M. Halverson, D. Winiarski, M. Rosenberg et al., "US Department of Energy commercial reference building models of the national building stock," 2011.

[21] J.-Y. Lee, A. Rahman, S. Huang, A. D. Smith, and S. Katipamula, "On-policy learning-based deep reinforcement learning assessment for building control eficiency and stability," Science and Technology for the Built Environment, vol. 28, no. 9, pp. 1150–1165, 2022.

[22] G. Van Rossum and F. L. Drake, Python 3 reference manual. CreateSpace, 2009.

[23] M. Wetter, P. Ehrlich, A. Gautier, M. Grahovac, P. Haves, J. Hu, A. Prakash, D. Robin, and K. Zhang, "OpenBuildingControl: Digitizing the control delivery from building energy modeling to specification, implementation and formal verification," Energy, vol. 238, p. 121501, 2022.

[24] M. Wetter, W. Zuo, T. S. Nouidui, and X. Pang, "Modelica buildings library," Journal of Building Performance Simulation, vol. 7, no. 4, pp. 253–270, 2014.

[25] X. Lu, Y. Fu, Z. O'Neill, and J. Wen, "A holistic fault impact analysis of the high-performance sequences of operation for HVAC systems: Modelica-based case study in a medium-ofice building," Energy and Buildings, vol. 252, p. 111448, 2021.

[26] K. Zhang, D. Blum, H. Cheng, G. Paliaga, M. Wetter, and J. Granderson, "Estimating ASHRAE Guideline 36 energy savings for multi-zone variable air volume systems using Spawn of EnergyPlus," Journal of Building Performance Simulation, vol. 15, no. 2, pp. 215–236, 2022.

[27] M. Wetter, K. Benne, and B. Ravache, "Software Architecture and Implementation of Modelica Buildings Library Coupling for Spawn of EnergyPlus," in Modelica Conferences, 2021, pp. 325–334.

[28] F. Engdahl and D. Johansson, "Optimal supply air temperature with respect to energy use in a variable air volume system," Energy and Buildings, vol. 36, no. 3, pp. 205–218, 2004.

[29] C. Y. H. Chao and J. Hu, "Development of a dual-mode demand control ventilation strategy for indoor air quality control and energy saving," Building and Environment, vol. 39, no. 4, pp. 385–397, 2004.

[30] H. S. Asad, R. K. K. Yuen, and G. Huang, "Multiplexed real-time optimization of HVAC systems with enhanced control stability," Applied Energy, vol. 187, pp. 640–651, 2017.

[31] M. Wetter, K. Benne, A. Gautier, T. S. Nouidui, A. Ramle, A. Roth, H. Tummescheit, S. Mentzer, and C. Winther, "Lifting the garage door on Spawn, an open-source BEM-controls engine," in In Proceedings of the 2020 Building Performance Modeling Conference and SimBuild co-organized by ASHRAE and IBPSA-USA, 2020.

[32] ASHRAE, "Standard 62.1 Ventilation for Acceptable Indoor Air Quality," American Society of Heating, Refrigerating and Air-Conditioning Engineers, 2019.

[33] Department of Energy, "Commercial Reference Buildings," https://www.energy.gov/eere/buildings/commercial-reference-buildings.

[34] ASHRAE, "Handbook applications," ASHRAE, Atlanta, 2003.

[35] R.P. Fedder Industrial, "MERV 13 Air Filters," 2022. [Online]. Available: https://www.rpfedder.com/filtration/merv-13-filters/

[36] C. A. Faulkner, J. E. Castellini Jr, W. Zuo, D. M. Lorenzetti, and M. D. Sohn, "Investigation of HVAC operation strategies for ofice buildings during COVID-19

pandemic," Building and Environment, vol. 207, p. 108519, 2022.

[37] ASHRAE, "Standard 52.2. Method of Testing General Ventilation Air-Cleaning Devices for Removal Eficiency by Particle Size," American Society of Heating, Refrigerating and Air-Conditioning Engineers, 2017.

[38] C. A. Faulkner, J. E. Castellini Jr, Y. Lou, W. Zuo, D. M. Lorenzetti, and M. D. Sohn, "Tradeoffs among indoor air quality, financial costs, and $CO2$ emissions for HVAC operation strategies to mitigate indoor virus in US ofice buildings," Building and Environment, vol. 221, p. 109282, 2022.

[39] G. Buonanno, L. Stabile, and L. Morawska, "Estimation of airborne viral emission: Quanta emission rate of SARS-CoV-2 for infection risk assessment," Environment International, vol. 141, p. 105794, 2020.

[40] G. Buonanno, L. Morawska, and L. Stabile, "Quantitative assessment of the risk of airborne transmission of SARS-CoV-2 infection: prospective and retrospective applications," Environment International, vol. 145, p. 106112, 2020.

[41] L. F. Pease, N. Wang, T. I. Salsbury, R. M. Underhill, J. E. Flaherty, A. Vlachokostas, G. Kulkarni, and D. P. James, "Investigation of potential aerosol transmission and infectivity of SARS-CoV-2 through central ventilation systems," Building and Environment, vol. 197, p. 107633, 2021.

[42] A. Persily and L. de Jonge, "Carbon dioxide generation rates for building occupants," Indoor Air, vol. 27, no. 5, pp. 868–879, 2017.

[43] E. Riley, G. Murphy, and R. Riley, "Airborne spread of measles in a suburban elementary school," American Journal of Epidemiology, vol. 107, no. 5, pp. 421–432, 1978.